 CMC, vol.35, no.3, pp.255-283, 2013

A Damage-Mode Based Three Dimensional Constitutive Model for Fibre-Reinforced Composites

M. Chatiri[1], **A. Matzenmiller**[2]

Abstract: This article presents a three dimensional constitutive model for anisotropic damage to describe the elastic-brittle behavior of unidirectional fibre-reinforced laminated composites. The primary objective of the article focuses on the three dimensional relationship between damage of the material and the effective elastic properties for the purpose of stress analysis of composite structures, in extension to the two dimensional model in Matzenmiller, Lubliner and Taylor (1995). A homogenized continuum is adopted for the constitutive theory of anisotropic damage and elasticity. Damage initiation criteria are based on Puck failure criterion for first ply failure and progressive micro crack propagation is based on the idea of continuum damage evolution. Internal variables are introduced to describe the evolution of the damage state under loading and as a subsequence the degradation of the material stiffness. Emphasis is placed on a suitable coupling among the equations for the rates of the damage variables with respect to the different damage modes.

Keywords: Three dimensional (3D) damage model, Fibre-reinforced laminated composites, Anisotropic damage, Damage rates equations, Internal variables, Damage mechanics, Damage modes, First-ply failure, Dissipation potential, Puck's criterion

1 Introduction

Damage plays a vital role in many fibre-reinforced composite (FRC) materials with non-ductile matrices. Their elastic brittle behavior is characterized by the formation and evolution of microcracks (surface discontinuities) and cavities (volume discontinuities). The pronounced irreversibility of these defects is a consequence. These defects primarily cause stiffness degradation and only small permanent deforma-

[1] CADFEM GmbH, Grafing/Munich, Germany. Email: mchatiri@cadfem.de

[2] Prof., Dept. of Mech. Engineering, Univ. of Kassel, Kassel, Germany. Email: post-structure@uni-kassel.de

tions remain in the stress-free body after unloading as long as the material is not close to complete deterioration. The main objective of this paper is the generation of a damage model for the numerical stress analysis of FRC structures.

Failure criteria are not sufficient to predict the progressive failure of composite structures which can accumulate damage before structural collapse. Simplified models, such as the ply discount method, can be used to indicate the onset of ultimate failure. But they cannot represent with satisfactory accuracy the process of brittle failure of laminates resulting from the accumulation of several failure mechanisms. The study of the non-linear response of brittle materials due to the accumulation of damage is important because the rate and direction of damage propagation define the damage tolerance of a structure and its eventual collapse, see Maimí, Camanho, Mayugo, and Dávila (2007). To model the phenomena of damage propagation, non-linear constitutive models, defined in the context of the mechanics of continuous media, have been developed and implemented into finite elements codes in recent years, see Pinho, Iannuci, and Robinson (2005), Williams, Vaziri, and Poursartip (2003). The formalism of the thermodynamics of irreversible processes serves as a guideline from which the constitutive models may be developed, see Lubliner (1990).

The simplest way to describe damage is by using a single scalar damage variable, as proposed by Kachanov, see Kachanov (1958). Damage can be interpreted as the creation of microcavities and microcracks with the damage variable as a measure of the effective surface density of the microdefects. Such a mechanical interpretation of damage assumes that the loads are resisted only by the undamaged ligaments in the material. The stresses $\widehat{\boldsymbol{\sigma}}$ in the ligaments, referred to as effective stresses, continue to increase until all ligaments are severed and the ply has failed. The tensorial representation of damage is a formal and general procedure in continuum damage mechanics (CDM) to represent the directionality of microcracks, which can take any direction in a homogenous medium depending on the load history, geometry, boundary conditions, and material properties. After Kachanov's pioneering work, several damage models that describe damage as a second, see Chaboche (1995), or as a fourth–order tensor, see Simo and Ju (1987a, 1987b) have been developed. Second order tensors describe an initially isotropic material as an orthotropic one when damage evolves, whereas fourth-order tensor models can remove all material symmetries and provide a more general procedure to simulate damage, see Cauvin and Testa (1999). The reduction of the elastic properties of a cracked ply predicted using continuum damage mechanics model can also be seen in Talreja's work, see Talreja (1985a, 1985b).

The application of continuum damage models to orthotropic or transversely isotropic materials, such as FRC, results in additional difficulties. The nature and

morphology of the material induce some preferred directions for crack growth, i.e., crack orientations are induced not only by the loads, geometry and boundary conditions, but also by the morphology of the material. The interface between fibre and matrix is weaker than the surrounding material and interfacial debonding is normally the first damage mechanism to occur. Furthermore, residual micromechanical thermal stresses are initiated in the composite plies due to different coefficients of the thermal expansion of the fibre and matrix. Multiscale analysis and mesomodeling are two approaches used to evaluate the elastic and inelastic response of a heterogeneous material. By using homogenization methods, multiscale models define relations between a mesoscale, which is normally the scale of the finite elements, where the material is considered as homogeneous, and the microscale, which is the level of fibre and matrix constituents. The constitutive models are either defined at the microscale and solved analytically, where strain or stress fields are related to the ones of the mesoscale by transformation field tensors, denoted as concentration tensors or the representative volume element (RVE) is analyzed numerically using finite elements, see Kurnatowski (2010), Kurnatowski and Matzenmiller (2012). To reduce the amount of computations that need to be performed, periodicity of the material is invoked.

Mesomodeling is an alternative way to set up damage models for composite materials in the case of large scale computations. Mesomodels treat the composite lamina, see Matzenmiller, Lubliner and Taylor (1995), or sub-laminate, see Williams, Vaziri, and Poursartip (2003) as a homogeneous substitute material. When diffuse damage localizes in a narrow band and becomes a macrocrack, the response is dominated by the crack tip formation and its ability to dissipate energy. On the other hand, the material's morphology, which is the main basis of homogenization techniques, loses importance for local failure analysis due to the loss of periodicity. Therefore, in structures exhibiting stable crack propagation, i.e. when the stresses increase monotonically with strain, mesomodeling is more appropriate than multiscale analysis for predicting the structural response up to collapse.

Based on the growing reliability of in-plane failure prediction, the application of FRC has been extended to complex geometries including primary load transferring components, in light weight design. An efficient design of such materials and structures requires a reliable failure prediction system under the general three dimensional (3D) states of stress. Puck's action-plane related failure criteria which are 3D formulations, see Puck and Schürmann (2004), along with post failure degradation procedures based on continuum damage mechanics as in Matzenmiller, Lubliner and Taylor, (1995), Ladeveze, Allix, Deü and Leveque (2000) are promising to predict lamina failure and post failure load redistribution in multidirectional laminates. In the present work, the prediction of laminate failure is treated within the

framework of “first ply failure” based on the Puck’s failure criterion and progressive damage based on the idea of continuum damage mechanics. The laminate is a stack of laminae of different fibre orientations. An explicit finite element analysis is applied to laminates and the material model formulation is developed at the unidirectional (UD-) lamina level. A homogenized continuum provides the theoretical basis for the constitutive model of each UD-lamina. The orthotropic nature of the lamina as a homogenized continuum with invariant axes of symmetry planes is maintained throughout the entire damaging process in the model. Linear elastic unloading and no plastic (irreversible) deformations are assumed to occur. Damage activation functions, based on the Puck failure criterion, are used to predict the different failure mechanisms occurring at the ply level.

This article is organized as follows. First, the mechanical behavior of laminated FRC materials is outlined in section 2. Glass- or carbon-fibre reinforced vinylester or epoxy resin falls into this class of materials. Special emphasis is given to the interaction between fibre damage due to fibre stress and matrix damage due to transverse and shear stresses on the basis of the elastic response and the ability to transmit various states of stresses. As an outgrowth of various failure mechanisms, also denoted as failure modes for fibre-composites in section two, the loading surfaces in strain space for UD-laminae are obtained by identifying them with the corresponding failure surfaces in stress space, see sections three and four. A set of "internal variables", denoted as damage variables, are introduced to indicate the state of anisotropic damage within the limits of the theory for "homogenized continua". These unknowns are treated as phenomenological internal variables, since they have no direct relation to the micromechanics of crack and void growth.

A simple algebraic structure of the constitutive tensor for the damaged lamina is proposed in section three. Its dependence on the damage variables gives rise to the application of the theory of internal variables for irreversible mechanical processes. It provides the necessary kinetic equations for the “internal (hidden) variables” of the damaged material. For this purpose, a potential function - denoted as the damage potential or dissipation potential - is introduced mainly for convenience.

The Kelvin inequality of thermodynamics, poses well-known restrictions on possible candidates for the dissipation potential. The second law of thermodynamics is assumed to hold for the proposed set of internal variables, despite the fact that the list might be incomplete. Nonnegative dissipation, however, must be a necessary ingredient for any constitutive model if the internal energy production shall be non-negative. A family of growth relations is suggested next (see section 5) to complete the "rate-independent" kinetic equations. Numerical examples for parameter identification, verification and validation finally conclude this paper describing a constitutive model with failure mechanisms (intralaminar failure: matrix cracks

and fibre fractures) to predict the onset and propagation of intralaminar damage in laminated composites.

2 Failure mechanisms of fibre reinforced composites

The model, proposed for laminated composites in this work, predicts the intralaminar failure mechanisms of matrix cracking in tension, compression, and shear as well as fibre fracture in tension or compression, see Hashin (1980). The concept of intralaminar damage modes is an extension of Hashin's fibre failure (FF) and Puck's interfibre failure (IFF) criterion. The interfacial damage (interlaminar failure) or delamination of individual layers is typically a failure form of the laminate and their mathematical modeling is a task beyond the scope of this topic. Intralaminar failure mechanisms trigger structural collapse of unidirectional laminates almost immediately. In matrix-dominated failure modes, collapse of the UD-laminate as a stack of laminae with same direction angle occurs as soon as a matrix crack is created. Failure of unidirectional laminates loaded in the longitudinal (fibre) direction, results from the accumulation of fibre fractures, see Rosen and Dow (1972).

However, multidirectional laminates can sustain increasing amounts of intralaminar failure mechanisms before structural collapse occurs. Considering the multidirectional laminate under uniform loading as a representative volume element, the intralaminar failure mechanisms can be regarded as damage mechanisms, i.e. distributed microcracks in a laminate whose tangent stiffness tensor still remains positive definite. When the tangent stiffness tensor of the laminate ceases to be positive definite, a macrocrack is formed and structural collapse ensues, see Maimí, Camanho, Mayugo, and Dávila (2007).

The main characteristics of the failure mechanisms occurring in laminated composites are briefly described in the following sections. These characteristics are the basis for the definition of the failure criteria and damage variables used in this work.

2.1 Fibre failure (FF) or longitudinal failure

Stresses in fibre direction are predominantly transmitted through the fibres because of their high stiffness and strength in comparison with the properties of the matrix material. The transmission of tensile stresses in the fibres is hardly impaired by the state of damage in the matrix, since fibres straighten under high tension. The straightening of the fibres may contribute to matrix damage in the absence of fibre rupture. The load carrying capacity of fibres in compression, however, is severely affected by the effective stiffness and strength of the surrounding matrix phase. The matrix acts like an "elastic foundation" for the fibres, treated in mechanical models

as beams under compression. Both, fibre rupture due to tension, and buckling or kinking of fibres due to compression cause damage evolution in resin matrices. As a consequence, all stiffness components of the constitutive tensor for the damaged unidirectional lamina are typically degraded.

As explained above, fibre fracture is primarily caused by the stress σ_{11} which acts parallel to the fibres. It expresses the physical idea that fibre fracture under a multiaxial state of stress in a UD-lamina occurs when its stress parallel to the fibres σ_{11} is equal to or exceeds the stress necessary for fracture. The simple Puck FF-condition follows from this hypothesis, see Hashin (1980), Knops (2008), Puck and Schürmann (2004), Deuschle and Kröplin (2012). It describes by case distinction the tensile fibre mode

$$\text{for} \quad \sigma_{11} \geq 0: \quad f^{+}_{\text{E,FF}} = \left(\frac{\sigma_{11}}{R^{+}_{\parallel}} \right)^2 - 1 \begin{cases} \geq 0 \text{ failed} \\ < 0 \text{ elastic} \end{cases} \tag{1}$$

and the compressive fibre mode

$$\text{for} \quad \sigma_{11} < 0: \quad f^{-}_{\text{E,FF}} = \left(\frac{\sigma_{11}}{R^{-}_{\parallel}} \right)^2 - 1 \begin{cases} \geq 0 \text{ failed} \\ < 0 \text{ elastic} \end{cases} \tag{2}$$

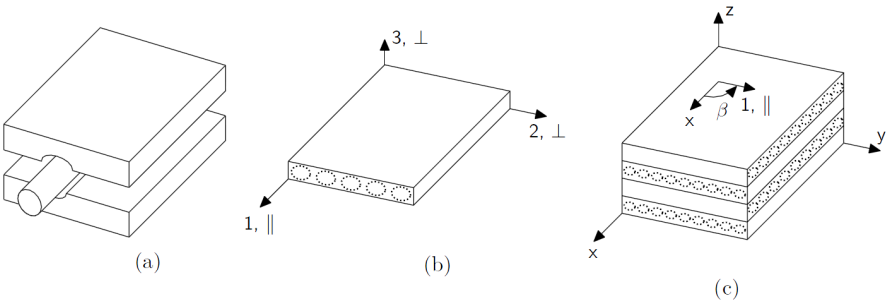

Figure 1: Definition of scales and coordinate system of UD-fibre reinforced composite: (a) micro-mechanical level, (b) lamina or meso level and (c) laminate level

wherein $R^{+}_{\parallel}$, $R^{-}_{\parallel}$ denote the corresponding material strength parameters. The coordinate system used above is according to the Fig. 1. It can be seen that a simple maximum stress criteria is used for fibre compressive failure which is generally approved by extensive experimental work, see Fischer (2003). More sophisticated fibre fracture criteria, see Fischer (2003), Puck and Schürmann (2004), Pinho, Iannuci, and Robinson (2005) which describe the influence of transverse and shear stresses, are not used in the present work due to lack of experimental data.

2.2 Inter-fibre failure (IFF) or transverse failure

Normal stresses, acting transverse to the fibres and shear stresses are transmitted through both matrix and fibres. However, their damaging effect mainly takes place in the matrix or in the fibre-matrix interface, leading to debonding. Usually, the bond strength of the interface zone between fibres and matrix is the lowest in comparison to the data for the strength of the single constituents. Advancing cracks in the matrix soon pass into the fibre-matrix interface and propagate along the fibres without crossing into the fibre material. Progressive opening of existing cracks is characteristic for tensile loading in transverse direction, whereas "crushing" in the sense of "fragmentation" of brittle matrix materials is very typical for compression in transverse direction. Under impact loading, brittle materials completely crumble or pulverize in extreme cases. Following the FF, see Fig. 2a. and IFF, see Fig. 2c, 2d, 2e, observations outlined above, the failure modes considered in the model proposed here are schematically represented in Fig. 2.

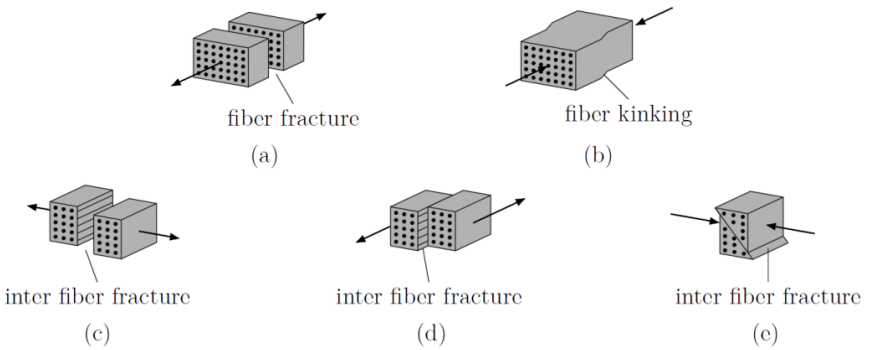

Figure 2: Major failure modes considered in the model as in Knops (2008)

Experimental results have shown that moderate values of transverse compression have a beneficial effect on the strength of a ply, see Soden, Hinton and Kaddour (2004): when the in-plane shear stress is large, compared to the transverse compressive stress, the fracture plane is perpendicular to the mid-plane of the ply. However, increasing the compressive transverse stress causes a change in the angle of the fracture plane. Normally, for carbon–epoxy and glass–epoxy composites, loaded in pure transverse compression, the fracture plane is at an angle (fracture angle) of $53^\circ \pm 3^\circ$, see Puck and Schürmann, (1998). Therefore, matrix cracking does not occur in the plane of the maximum transverse shear stress under the angle of 45°.

For the above described transverse failure, the Puck IFF criteria are most promising

for brittle, plastic unidirectional (UD) laminates - see Fig. 3. The UD-ply behaves transversely isotropic in both cases, elasticity and failure. Puck assumes a Mohr–Coulomb type of failure criterion for loading transverse to the fibre direction. Failure is assumed to be caused by the normal and shear components operating on the action plane of stresses $\sigma_n,\ \tau_{n1},\ \tau_{nt}$ - see Fig. 3 and Hashin (1980). Positive normal stress on this plane promotes fracture while a negative one increases the material's shear strength, thus, impeding fracture. Puck's stress based failure criteria enable the computation of the material exposure $f_{\mathrm{E,IFF}}(\theta)$ as a failure indicator, wherein θ is the orientation angle.

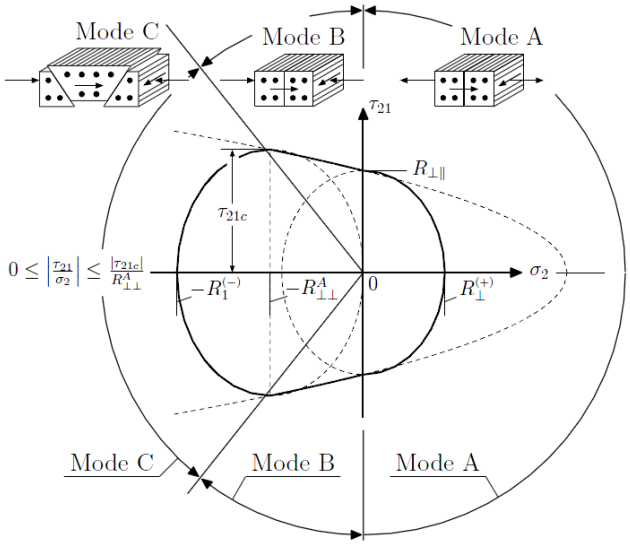

Figure 3: Schematic representation of failure modes and failure plane based on Puck, as in Knops (2008)

The 3D Puck failure criterion can be categorized as below in Tab. 1 in extension to Fig. 3.

The values of $f_{\mathrm{E,IFF}}(\theta)$ range between 0, where the material is unstressed, and up to 1, denoting the onset of IFF. The material exposure $f_{\mathrm{E,IFF}}(\theta)$ is a function of the stress state $\boldsymbol{\sigma}$ and the orientation angle θ of the stress action plane with respect to the transverse direction $\mathbf{X}_2$ as in Fig. 5 right. The fracture plane stresses are obtained by rotating the three dimensional stress tensor from material coordinates to the preferred axes of the fracture plane, designated also as the action plane of stresses. The master failure surface on the fracture plane is defined in terms of

Table 1: Categorization of fracture modes in failure criteria of Puck under three dimensional stress states

Fracture angle	Sign of σ_n	Fracture mode
90°	positive	Delamination
0° to 89°	positive	A
−53° to 0°	negative	B
−90° to −53°	negative	C

the Mohr-Coulomb stresses, thus, yielding the following failure criteria by case distinction in tension and compression:

for: $\sigma_n \geq 0$:

$$f^{+}_{\mathrm{E,IFF}}(\theta) = \sqrt{\left[\frac{1}{R^{+}_{\perp}} - \frac{p^{+}_{\perp\psi}}{R^{A}_{\perp\psi}}\right]^2 [\sigma_n(\theta)]^2 + \left[\frac{\tau_{nt}(\theta)}{R^{A}_{\perp\perp}}\right]^2 + \left[\frac{\tau_{n1}(\theta)}{R_{\perp\parallel}}\right]^2} + \frac{p^{+}_{\perp\psi}}{R^{A}_{\perp\psi}}\sigma_n(\theta) - 1 \tag{3}$$

and

for: $\sigma_n < 0$:

$$f^{-}_{\mathrm{E,IFF}}(\theta) = \sqrt{\left[\frac{\tau_{nt}(\theta)}{R^{A}_{\perp\perp}}\right]^2 + \left[\frac{\tau_{n1}(\theta)}{R_{\perp\parallel}}\right]^2 + \left[\frac{p^{-}_{\perp\psi}}{R^{A}_{\perp\psi}}\sigma_n(\theta)\right]^2} + \frac{p^{-}_{\perp\psi}}{R^{A}_{\perp\psi}}\sigma_n(\theta) - 1 \tag{4}$$

The only unknown parameters in these equations are $p^{\pm}_{\perp\psi}$, $R^{A}_{\perp\psi}$, and $R^{A}_{\perp\perp}$ which depend on the shear stresses τ_{nt} and τ_{n1} according to the following equations:

$$\frac{p^{\pm}_{\perp\psi}}{R^{A}_{\perp\psi}} = \frac{p^{\pm}_{\perp\perp}}{R^{A}_{\perp\perp}} \frac{\tau^2_{nt}}{\tau^2_{nt} + \tau^2_{n1}} + \frac{p^{\pm}_{\perp\parallel}}{R_{\perp\parallel}} \frac{\tau^2_{n1}}{\tau^2_{nt} + \tau^2_{n1}} \tag{5}$$

and

$$R^{A}_{\perp\perp} = \frac{R^{-}_{\perp}}{2(1 + p^{-}_{\perp\perp})} \tag{6}$$

wherein $R^{+}_{\perp}$, $R_{\perp\parallel}$, $R^{-}_{\perp}$ denote the corresponding material strength parameters, and $p^{\pm}_{\perp\perp}$, $p^{\pm}_{\perp\parallel}$ are constants introduced by Puck, see Puck and Schürmann (2004). The action plane with the greatest failure effort $f_{\mathrm{E}}(\theta)$ (wherein $\theta = -90°$ to $+90°$) is the fracture plane to be expected, $[f_{\mathrm{E}}(\theta)]_{\mathrm{MAX}} = f_{\mathrm{E}}\big|_{\theta=\theta_{\mathrm{fp}}}$. Once the failure plane

with max $f_{\mathrm{E}}(\theta)$ is found, the fracture angle as θ_{fp} is kept constant in the model and progressive failure, based on the idea of continuum damage, is applied to the material model for the corresponding lamina at hand, see below.

The failure criteria may be interpreted as loading criteria, a terminology encountered in strain space plasticity. The role played by the yield stress in plasticity will be taken by the threshold variables r_i in damage mechanics. As proposed by Kachanov in classical continuum damage mechanics, only the undamaged (whole) part of the cross-section A (net-area) for the uniaxial case is supposed to carry loading, i.e. transmit stresses. Consequently, the stresses σ_{ij} in the failure criteria should be interpreted as effective stresses $\hat{\sigma}_{ij}$, referred to the net area. This means that the failure criteria are assumed to hold in terms of the effective stresses rather than the nominal ones.

2.3 Interlaminar failure (Delamination)

As described earlier, a laminate as a stacked composition of several laminae may fail by the separation of two or more of its layers. Such a delamination process is caused by inter-laminar stresses acting on the interface namely through-thickness tension, and inplane or through-thickness shear. However, delamination modeling is a task beyond the scope of this paper.

2.4 Qualitative example showing progressive failure of cross ply laminates

The failure of a composite material is a sequence of the described individual but interacting failure mechanisms. The progressive damage of a symmetric $[0^\circ/90^\circ/90^\circ/0^\circ]$ laminate loaded in the y-direction (see Fig. 4) is representative for the complex and interacting failure process of UD-fibre reinforced composites. Loaded in-plane by a tensile force, the first damage occurs in the 0°-laminae where the fibre-transverse tensile stress $\sigma^t_{22\perp}$ produces first ply failure in form of vertical micro-cracks, IFFs ($\theta_{\mathrm{fp}} = 0^\circ$). Increasingly loaded, the 0°-laminae develop more and more IFFs (see Fig. 4a) going along with the decrease of the stiffness – denoted as the degradation of these laminae. The result is a load redistribution from the damaging laminae to the neighbouring ones. Accordingly, the tensile stress $\sigma^t_{11\parallel}$ in the 90°-laminae increases together with the laminae's lateral contraction known as POISSON's effect. Impeded by the fibres of the 0°-laminae (they carry compressive $\sigma^c_{11\parallel}$), the result is a fibre-transverse tension $\sigma^t_{22\perp}$ in the 90°-laminae producing the second ply failure: vertical IFFs in the 90°-laminae, see Fig. 4b. Still capable of bearing load, the laminate may be increasingly stressed until the following fibre fractures in the 90°-laminae mark the third ply failure and the final breakdown of the laminate, see Fig. 4c. This example proves the importance of the distinction between fibre failure (FF) and inter-fibre failure (IFF) regarding the

progressive failure analysis in a damage-tolerant design process.

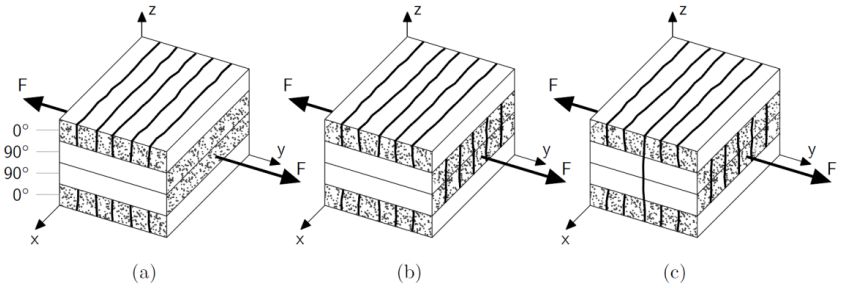

Figure 4: Section of a laminate $[0°/90°/90°/0°]$ under increasing load: (a) first ply failure IFFs in the 0°-laminae, (b) second ply failure IFFs in the 90°-laminae and (c) third ply failure FFs in the 90°-laminae

3 Damage variables, effective stresses and compliance tensor

3.1 Damage variables and the concept of effective stresses

As already indicated at the outset, the orthotropic nature of the mechanical response is maintained at all states of damage for treating the lamina as a homogenized continuum. This assumption permits the modeling of damage by macro cracks coinciding with the failure planes as in Fig. 2. The orientation of each set of cracks for fibre and interfibre damage is given by the unit normal vector $\mathbf{n}$, also denoted as damage normal. A nonnegative scalar valued damage variable ω is introduced, which measures the degradation of the elastic material properties as stiffness loss or flexibility increase. It may be identified as the void area density. The damage vector $\boldsymbol{\varpi}$ may be defined as:

$$\boldsymbol{\varpi}=\omega\mathbf{n} \tag{7}$$

By considering two different arrays of oriented cracks for FF and IFF, their normal $\mathbf{n}_{\mathrm{FF}}$ and $\mathbf{n}_{\mathrm{IFF}}$ need to be defined. The normal vector $\mathbf{n}_{\mathrm{IFF}}$ which is perpendicular to the fracture plane, see Fig. 5 right, is then defined in the fracture plane coordinate system $(\mathbf{X}_1, \mathbf{X}_{\mathrm{n}}, \mathbf{X}_{\mathrm{t}})$ as:

$$\mathbf{n}_{\mathrm{IFF}} = \begin{bmatrix} 0 \\ 1 \\ 0 \end{bmatrix} \tag{8}$$

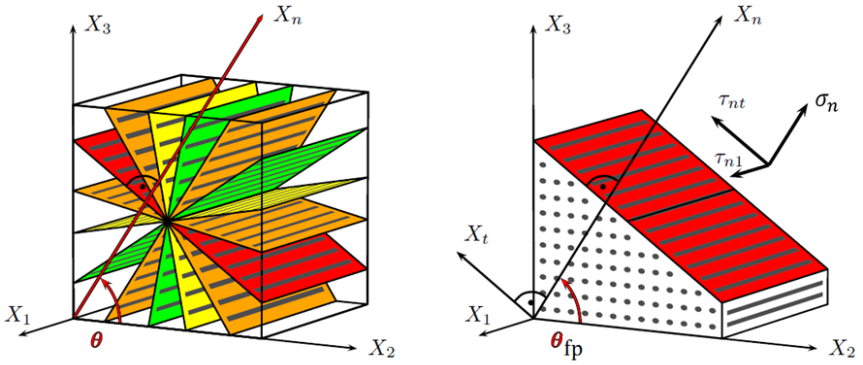

Figure 5: left: Action plane with max IFF in laminae coordinate system ($\mathbf{X}_1$, $\mathbf{X}_2$, $\mathbf{X}_3$) and right: Coordinate system ($\mathbf{X}_1$, $\mathbf{X}_n$, $\mathbf{X}_t$) on Inter-fibre fracture plane as in Knops (2008)

This vector, if transformed to the lamina coordinate system, with the orthogonal transformation matrix $\mathbf{T}$ from fracture plane coordinates ($\mathbf{X}_1$, $\mathbf{X}_n$, $\mathbf{X}_t$) to lamina coordinates ($\mathbf{X}_1$, $\mathbf{X}_2$, $\mathbf{X}_3$) can be written as:

$$\mathbf{n}_\perp = \mathbf{T}\mathbf{n}_{\text{IFF}} = \begin{bmatrix} 0 \\ \cos\theta_{\text{fp}} \\ \sin\theta_{\text{fp}} \end{bmatrix} \tag{9}$$

Similarly, the transverse damage vector is defined as:

$$\boldsymbol{\varpi}_\perp = \omega_{\text{IFF}} \begin{bmatrix} 0 \\ \cos\theta_{\text{fp}} \\ \sin\theta_{\text{fp}} \end{bmatrix} \tag{10}$$

For IFFs with vertical microcracks, it is $\theta_{\text{fp}} = 0$. Hence substituting the same in Eq. 10 yields:

$$\boldsymbol{\varpi}_\perp = \omega_{\text{IFF}} \begin{bmatrix} 0 \\ 1 \\ 0 \end{bmatrix} \tag{11}$$

If the degradation is described in the sense of CAUCHY's stress concept, six different non-negative damage parameters ω_{11}, ω_{22}, ω_{33}, ω_{12}, ω_{23} and ω_{13} are defined to quantify the relative size of macro cracks projected onto the coordinate planes, and assembled in the rank-four damage operator $\mathbf{M}$ given in VOIGT notation of Eq.

13d. In CDM, the effective normal stresses $\hat{\boldsymbol{\sigma}}$ are related to the damage parameters ω_{ij}, since only the undamaged part of the cross section A for the uniaxial case is supposed to carry loading. Consequently, the stresses σ_{ij} in the failure criteria should be interpreted as effective stresses $\hat{\sigma}_{ij}$, referred to the net area. A simple relationship between effective stress $\hat{\boldsymbol{\sigma}}$ and the nominal one $\boldsymbol{\sigma}$ holds:

$$\hat{\boldsymbol{\sigma}} = \mathbf{M}\boldsymbol{\sigma} \tag{12}$$

Wherein $\mathbf{M}$ represents the rank-four (uncoupled) damage operator given in VOIGT notation as:

$$\boldsymbol{\sigma} = \begin{bmatrix} \sigma_{11} \\ \sigma_{22} \\ \sigma_{33} \\ \tau_{12} \\ \tau_{23} \\ \tau_{13} \end{bmatrix}, \; \hat{\boldsymbol{\sigma}} = \begin{bmatrix} \hat{\sigma}_{11} \\ \hat{\sigma}_{22} \\ \hat{\sigma}_{33} \\ \hat{\tau}_{12} \\ \hat{\tau}_{23} \\ \hat{\tau}_{13} \end{bmatrix}, \; \boldsymbol{\omega} = \begin{bmatrix} \omega_{11} \\ \omega_{22} \\ \omega_{33} \\ \omega_{12} \\ \omega_{23} \\ \omega_{13} \end{bmatrix},$$

$$\mathbf{M} = \begin{bmatrix} \frac{1}{1-\omega_{11}} & 0 & 0 & 0 & 0 & 0 \\ 0 & \frac{1}{1-\omega_{22}} & 0 & 0 & 0 & 0 \\ 0 & 0 & \frac{1}{1-\omega_{33}} & 0 & 0 & 0 \\ 0 & 0 & 0 & \frac{1}{1-\omega_{12}} & 0 & 0 \\ 0 & 0 & 0 & 0 & \frac{1}{1-\omega_{23}} & 0 \\ 0 & 0 & 0 & 0 & 0 & \frac{1}{1-\omega_{13}} \end{bmatrix} \tag{13a-d}$$

3.2 Constitutive tensor of damaged UD-laminae

The nonlinear elasticity behavior for in-plane shear is modelled according to the Ramberg-Osgood type of material equation $\varepsilon = \frac{\sigma}{E} + \frac{\sigma_0}{E}\left(\frac{\sigma}{\sigma_0}\right)^n$ with elastic modulus E, stress like material parameter σ_0, POISSON's ratio υ and exponent n for the degree of non-linearity, see Ramberg and Osgood (1943).

In the undamaged state, a lamina behaves equally in the transverse 2-direction and the through-thickness 3-direction which allows to reduce the general anisotropy to a transversely isotropic behavior with only a fibre-parallel $\parallel$ (1) and fibre-perpendicular $\perp$(2) direction, see Fig. 1b. The constitutive behavior, i.e. the material equation relating, states of stress to states of strain, is then defined by the transversely isotropic compliance matrix $\mathbf{S}$ in VOIGT notation for the UD-laminae prior to the damage initiation, see Eq. 13. As discussed above, only the in-plane shear modulus $G_{\parallel\perp}(\varepsilon_{12})$ is modelled according to Ramberg-Osgood type of non-

linear material equation.

$$\begin{bmatrix} \varepsilon_{11} \\ \varepsilon_{22} \\ \varepsilon_{33} \\ 2\varepsilon_{12} \\ 2\varepsilon_{23} \\ 2\varepsilon_{13} \end{bmatrix} = \begin{bmatrix} \frac{1}{E_{\parallel}} & -\frac{\nu_{\perp\parallel}}{E_{\perp}} & -\frac{\nu_{\perp\parallel}}{E_{\perp}} & 0 & 0 & 0 \\ -\frac{\nu_{\parallel\perp}}{E_{\parallel}} & \frac{1}{E_{\perp}} & -\frac{\nu_{\perp\perp}}{E_{\perp}} & 0 & 0 & 0 \\ -\frac{\nu_{13}}{E_{\parallel}} & -\frac{\nu_{\perp\perp}}{E_{\perp}} & \frac{1}{E_{\perp}} & 0 & 0 & 0 \\ 0 & 0 & 0 & \frac{1}{G_{\parallel\perp}(\varepsilon_{12})} & 0 & 0 \\ 0 & 0 & 0 & 0 & \frac{1}{G_{\perp\perp}} & 0 \\ 0 & 0 & 0 & 0 & 0 & \frac{1}{G_{\parallel\perp}} \end{bmatrix} \begin{bmatrix} \sigma_{11} \\ \sigma_{22} \\ \sigma_{33} \\ \sigma_{12} \\ \sigma_{23} \\ \sigma_{13} \end{bmatrix} \tag{14}$$

For the pure failure analysis of a UD-fibre reinforced composite, the transversely isotropic material description is generally adequate but within the post-failure degradation process the lamina starts to behave truly orthotropic if not completely anisotropic. After the onset of cracking, the lamina's elastic behavior is assumed to be orthotropic with obvious planes of symmetry and preferred axes ($\mathbf{X}_1, \mathbf{X}_2, \mathbf{X}_3$) as given in Fig. 5.

Instead of taking the elasticity constants themselves as unknowns, see Ortiz (1985) and Ju (1989), the components of the constitutive tensor are represented as functions of the vector $\boldsymbol{\omega}$, comprising all internal damage variables, and the material parameters of the undamaged lamina. The constitutive tensor $\mathbf{C}(\boldsymbol{\omega})$ is derived by physical arguments and information of the dependencies between effective elastic properties and individual damage variables. Generally, for a given arbitrary damage operator, the postulate of strain equivalence yields an unsymmetrical constitutive tensor, which should be rejected as a model for the elastic behavior. This hypothesis serves here as a first guidance together with physical arguments to set up the constitutive tensor $\mathbf{C}(\boldsymbol{\omega})$ for the damaged lamina. For the purpose of building the dependence on damage into the constitutive assumption, the compliance relationship is more easily accessible in order to relate the material parameters to the mechanical response in the coordinate system with preferred axes. The compliance relationship for orthotropic elasticity in terms of effective stresses $\hat{\boldsymbol{\sigma}}$ reads as:

$$\boldsymbol{\varepsilon} = \mathbf{H_0}\hat{\sigma},\ \mathbf{H_0} = \begin{bmatrix} \frac{1}{E_{11}} & -\frac{\nu_{21}}{E_{22}} & -\frac{\nu_{31}}{E_{33}} & 0 & 0 & 0 \\ -\frac{\nu_{12}}{E_{11}} & \frac{1}{E_{22}} & -\frac{\nu_{32}}{E_{33}} & 0 & 0 & 0 \\ -\frac{\nu_{13}}{E_{11}} & -\frac{\nu_{23}}{E_{22}} & \frac{1}{E_{33}} & 0 & 0 & 0 \\ 0 & 0 & 0 & \frac{1}{G_{12}(\varepsilon_{12})} & 0 & 0 \\ 0 & 0 & 0 & 0 & \frac{1}{G_{23}} & 0 \\ 0 & 0 & 0 & 0 & 0 & \frac{1}{G_{13}} \end{bmatrix},\ \boldsymbol{\varepsilon} = \begin{bmatrix} \varepsilon_{11} \\ \varepsilon_{22} \\ \varepsilon_{33} \\ 2\varepsilon_{12} \\ 2\varepsilon_{23} \\ 2\varepsilon_{13} \end{bmatrix} \tag{15a-c}$$

It is to be noted that Eq. (15b) is symmetric. Equations (12) and (15a) result in:

$$\boldsymbol{\varepsilon} = \boldsymbol{H_0}\hat{\boldsymbol{\sigma}} = \mathbf{H_0 M}\boldsymbol{\sigma} \tag{16}$$

The final relationship of the compliance tensor for the damaged laminae $\mathbf{H}(\boldsymbol{\omega})$takes the following form after POISSON's ratios $\nu_{12}(\boldsymbol{\omega})$and $\nu_{21}(\boldsymbol{\omega})$ are adjusted according to the qualitative arguments presented in Matzenmiller, Lubliner and Taylor (1995).

$$\mathbf{H}(\boldsymbol{\omega}) = \begin{bmatrix} \frac{1}{(1-\omega_{11})E_{11}} & -\frac{\nu_{21}}{E_{22}} & -\frac{\nu_{31}}{E_{33}} & 0 & 0 & 0 \\ -\frac{\nu_{12}}{E_{11}} & \frac{1}{(1-\omega_{22})E_{22}} & -\frac{\nu_{32}}{E_{33}} & 0 & 0 & 0 \\ -\frac{\nu_{13}}{E_{11}} & -\frac{\nu_{23}}{E_{22}} & \frac{1}{(1-\omega_{33})E_{33}} & 0 & 0 & 0 \\ 0 & 0 & 0 & \frac{1}{(1-\omega_{12})G_{12}(\varepsilon_{12})} & 0 & 0 \\ 0 & 0 & 0 & 0 & \frac{1}{(1-\omega_{23})G_{23}} & 0 \\ 0 & 0 & 0 & 0 & 0 & \frac{1}{(1-\omega_{13})G_{13}} \end{bmatrix} \tag{17}$$

As explained earlier, the orthotropic nature of the lamina as a homogenized continuum is maintained throughout the damaging process. The shear coupling terms are neglected. Therefore, the symmetry class of the UD-lamina remains the same for all states of damage. Its inverse always exits as long as the damage variables are less than one $(\omega_{ij} < 1)$. Hence, the material stiffness tensor is given by:

$$\mathbf{C}(\boldsymbol{\omega}) = [\mathbf{H}(\boldsymbol{\omega})]^{-1} \tag{18}$$

4 Loading surfaces and loading conditions

4.1 Loading criteria

The state of damage is unchanged along a path of strain in the interior of a well-defined region, called the elastic range $\boldsymbol{\mathcal{E}}$. Further, it is supposed that any state of stress or strain lies either inside $\boldsymbol{\mathcal{E}}$ or on the boundary $\partial\boldsymbol{\mathcal{E}}$ of the elastic range, defined by the loading criterion in stress space $f(\boldsymbol{\sigma},\ \boldsymbol{\omega},\ r)$or strain space $g(\boldsymbol{\varepsilon}, \boldsymbol{\omega}, r)$in terms of either $\boldsymbol{\sigma}$ or $\boldsymbol{\varepsilon}$ and the damage variables $\boldsymbol{\omega}$ as well as the threshold r . If the elastic range is bounded by several surfaces f_i or g_i, each surface can have its own threshold r_i. The vector of damage thresholds $\mathbf{r}$ measures the size of the elastic region. As it is assumed here, their evolution is governed by the consistency condition $\dot{g} = 0$, which relates the evolution of the thresholds $\mathbf{r}$ to the one for the damage variables assembled in $\boldsymbol{\omega}$. Therefore, the thresholds $\mathbf{r}$ are no longer independent internal variables.

After the stress components σ_{ij} in the failure criteria are formally replaced by the effective ones $\hat{\sigma}_{ij}$, the loading surfaces $f_1^{\pm}$ for the fibre mode (FF) and $f_2^{\pm}$ for the

matrix IFF mode are derived by making use of case distinctions:

$$\text{for } \sigma_1 \geq 0: \; f_1^+ = \frac{\sigma_{11}^2}{(1-\omega_{11}^+)^2 R_\parallel^{+2}} - r_1^+ = 0 \tag{19}$$

and

$$\text{for } \sigma_1 < 0: \; f_1^- = \frac{\sigma_{11}^2}{(1-\omega_{11}^-)^2 R_\parallel^{-2}} - r_1^- = 0, \tag{20}$$

Wherein r_1^+ and r_1^- are the threshold variables varying from 1 to ∞ for tension and compression.

The fibre loading criterion in stress space may also be written by case distinction as:

$$f_1^\pm = \boldsymbol{\sigma}^T \mathbf{F}_1^\pm \boldsymbol{\sigma} - r_1^\pm = 0, \tag{21}$$

wherein

$$\mathbf{F}_1^\pm = \begin{bmatrix} \left[(1-\omega_{11}^\pm)R_\parallel^\pm\right]^{-2} & 0 & 0 & 0 & 0 & 0 \\ 0 & 0 & 0 & 0 & 0 & 0 \\ 0 & 0 & 0 & 0 & 0 & 0 \\ 0 & 0 & 0 & 0 & 0 & 0 \\ 0 & 0 & 0 & 0 & 0 & 0 \\ 0 & 0 & 0 & 0 & 0 & 0 \end{bmatrix} \tag{22}$$

It is well known that the stress-strain relationship in softening branches of its graph is stable under strain control only. Hence for the transformation of f (stress space) into g (strain space), the constitutive tensor is employed to change the defining spaces.

For fibre failure (parallel) mode

$$\text{for } \sigma_1 \geq 0, \quad g_1^+ = \left(\frac{E_{11}\varepsilon_{11}}{(1-\omega_{11}^+)R_\parallel^+}\right)^2 - r_1^+ = 0 \tag{23}$$

and

$$\sigma_1 < 0, \quad g_1^- = \left(\frac{E_{11}\varepsilon_{11}}{(1-\omega_{11}^-)R_\parallel^-}\right)^2 - r_1^- = 0 \tag{24}$$

The above equations (Eq. 23 and Eq.24) may be written conveniently as:

$$g_i = \boldsymbol{\varepsilon}^T \mathbf{G}_i \boldsymbol{\varepsilon} - r_i = 0 \tag{25}$$

With $\mathbf{G}_i = \mathbf{C}\mathbf{F}_i\mathbf{C}$, wherein i = 1, 2 being the two different modes.
Similarly for the IFF matrix mode:

$$\text{for } \sigma_n \geq 0: \; f_2^+ = \sqrt{\left[\frac{1}{R_\perp^{(+)}} - \frac{p_{\perp\psi}^{(+)}}{R_{\perp\psi}^{(A)}}\right]^2 \sigma_n^2 + \left[\frac{\tau_{nt}}{R_{\perp\perp}^{(A)}}\right]^2 + \left[\frac{\tau_{n1}}{R_{\perp\parallel}}\right]^2} + \frac{p_{\perp\psi}^{(+)}}{R_{\perp\psi}^{(A)}}\sigma_n - r_2^+ = 0 \tag{26}$$

and

$$\text{for } \sigma_n < 0: \; f_2^- = \sqrt{\left[\frac{\tau_{nt}}{R_{\perp\perp}^{(A)}}\right]^2 + \left[\frac{\tau_{n1}}{R_{\perp\parallel}}\right]^2 + \left[\frac{p_{\perp\psi}^{(-)}}{R_{\perp\psi}^{(A)}}\sigma_n\right]^2} + \frac{p_{\perp\psi}^{(-)}}{R_{\perp\psi}^{(A)}}\sigma_n - r_2^- = 0. \tag{27}$$

$$\text{Also,} \quad g_2^\pm = \boldsymbol{\varepsilon}^T \mathbf{G}_2^\pm \boldsymbol{\varepsilon} - r_2^\pm = 0 \tag{28}$$

4.2 Loading conditions

The present model is derived within the framework of irreversible thermodynamics, see Lubliner (1990), Matzenmiller, Lubliner and Taylor (1995), with internal variables which provide a qualitative measure of the effects that randomly distributed microdefects exert on the macro parameters of a structure. The boundary $\partial\mathcal{E}$ in strain space moves (at least locally) "outwards" with increasing strains, if the strain rate forms an acute angle with the gradient $\nabla_{\boldsymbol{\varepsilon}} g_i$ at the given state of strain on the loading surface. The damage state changes under these conditions, called

loading:

$$g_i = 0 \text{ and } \frac{\partial g_i}{\partial \boldsymbol{\varepsilon}}\dot{\boldsymbol{\varepsilon}} > 0, \tag{29a}$$

neutral loading:

$$g_i = 0 \text{ and } \frac{\partial g_i}{\partial \boldsymbol{\varepsilon}}\dot{\boldsymbol{\varepsilon}} = 0, \tag{29b}$$

and unloading:

$$g_i = 0 \text{ and } \frac{\partial g_i}{\partial \boldsymbol{\varepsilon}}\dot{\boldsymbol{\varepsilon}} < 0. \tag{29c}$$

Besides the damage variables $\boldsymbol{\omega}$ and the damage thresholds $\mathbf{r} = \begin{bmatrix} r_1^\pm \\ r_2^\pm \end{bmatrix}$ no other internal variables have been introduced to describe the location of the loading surface in strain space. The origin is contained in the elastic range $\mathcal{E}$ at all states of

damage. Therefore, $\boldsymbol{\mathcal{E}}$ has to expand at least locally when its boundary moves $\partial\boldsymbol{\mathcal{E}}$ "outwards" during loading, and the time derivative of the damage threshold $\dot{\mathbf{r}}$ must be non-negative $\dot{\mathbf{r}} \geq 0$. The consistency condition in strain space has to provide a monotonically increasing threshold $\mathbf{r}$ for a meaningful loading surface $g = 0$ in strain space.

$$\dot{g}_i = \frac{\partial g_i}{\partial \boldsymbol{\varepsilon}} \dot{\boldsymbol{\varepsilon}} + \frac{\partial g_i}{\partial \boldsymbol{\omega}} \dot{\boldsymbol{\omega}} - \dot{r}_i = 0 \tag{30}$$

5 Kinetic assumption

Damage growth $\dot{\boldsymbol{\omega}} > 0$ will occur when the strain path crosses the updated damage surface $g_i - r_i$ and the strain increment has a non-zero component in the direction of the normal to the damage surface, i.e.

$$\sum_i \frac{\partial g_i}{\partial \boldsymbol{\varepsilon}} \dot{\boldsymbol{\varepsilon}} > 0. \tag{31}$$

For simplicity, no case distinctions are made in the following for the damage variables $\boldsymbol{\omega}$, for which it is possible to distinguish between active and passive states.

5.1 General form of damage rule

In the presence of strain softening, the rate of evolution for the damage $\dot{\boldsymbol{\omega}}(\boldsymbol{\sigma},\ \boldsymbol{\omega},\ \dot{\boldsymbol{\varepsilon}})$ is supposed to be locally controllable under the strain rate $\dot{\varepsilon}$. Under these conditions, the rate-equations are:

$$\dot{\boldsymbol{\omega}} = \sum_i \varphi_i \mathbf{q}_i = \varphi_1 \mathbf{q}_1 + \varphi_2 \mathbf{q}_2. \tag{32}$$

The scalar functions $\varphi_i(\boldsymbol{\sigma},\ \boldsymbol{\omega},\ \dot{\boldsymbol{\varepsilon}})$ are multiple damage functions which control the amount of growth and the vector-valued functions $\mathbf{q}_i(\boldsymbol{\sigma},\ \boldsymbol{\omega})$ represent multiple damage coupling vectors which accommodate the coupling of growth for the individual damage variables in the various damage modes. Also, φ_i must be linear in $\dot{\boldsymbol{\varepsilon}}$ for a rate-independent process, see Matzenmiller, Lubliner and Taylor (1995).

Growth functions

The strain increment $\dot{\boldsymbol{\varepsilon}}$dt indicates the direction of the loading path $\boldsymbol{\varepsilon}(t)$ as it wants to cross the loading surface $g = 0$ in strain space. The scalars $\phi_i \geq 0$ have to be associated with each loading direction $\dot{\boldsymbol{\varepsilon}}$ in relation to the orientation of the normal $\nabla_{\boldsymbol{\varepsilon}} g_i$ and must be in accordance with the loading conditions.

$$\dot{\varphi}_i = 0 \text{ if } g_i = f_i \leq 0. \tag{33}$$

The strain path is either in the interior of the elastic range $\mathcal{E}$ or comes into contact with the boundary $\partial\mathcal{E}$ to yield in case of loading:

$$\dot{\varphi}_i > 0 \text{ if } g_i = f_i = 0_+ \tag{34}$$

The strain path crosses the loading surface $f_i = g_i = 0$ is indicated by the "+" sign at the end of the criterion in Eq. 34. The strain increment has a non-zero component pointing into the direction of the gradient $\boldsymbol{\nabla}_{\boldsymbol{\varepsilon}} g_i$.

Without loss of generality, the interacting damage parameters $l_{\mathrm{IFF}\tau_{n1}}$ and $l_{\mathrm{IFF}\tau_{nt}}$ for the IFF damage mode are assembled in the coupling vector $\mathbf{q}_{\mathrm{IFF}}$ in the fracture plane coordinate system ($\mathbf{X}_1$, $\mathbf{X}_\mathrm{n}$, $\mathbf{X}_\mathrm{t}$):

$$\mathbf{q}_{\mathrm{IFF}} = \begin{bmatrix} 0 \\ 1 \\ 0 \\ l_{\mathrm{IFF}\tau_{n1}} \\ 0 \\ l_{\mathrm{IFF}\tau_{nt}} \end{bmatrix} \tag{35}$$

The coupling of the rate-equations for the fluxes $\dot{\boldsymbol{\omega}}$ is controlled by the vectors $\mathbf{l}_{\parallel}$ for FF and $\mathbf{l}_{\perp}$ for IFF, which may be different for tension and compression. The following proposal satisfies the physical aspects of interacting coupling variables for the FF coupling vector $\mathbf{q}_1$ in the lamina coordinate system ($\mathbf{X}_1$, $\mathbf{X}_2$, $\mathbf{X}_3$)

$$\mathbf{q}_1 = \mathbf{l}_{\parallel} = \begin{bmatrix} 1 \\ l_{\parallel\sigma_{22}} \\ l_{\parallel\sigma_{33}} \\ l_{\parallel\tau_{12}} \\ l_{\parallel\tau_{23}} \\ l_{\parallel\tau_{13}} \end{bmatrix} \tag{36}$$

The components $l_{\parallel\sigma_{22}}$, $l_{\parallel\sigma_{33}}$, $l_{\parallel\tau_{12}}$, $l_{\parallel\tau_{23}}$, $l_{\parallel\tau_{13}}$ indicate coupling of the damage variables ω_{22}, $\omega_{33}, \omega_{12}, \omega_{23}$, ω_{13} for matrix cracking due to progressive fibre breakage damage variable ω_{11}. They may be estimated from experimental observations and according to the various failure modes of Puck, see Fig. 2. and Fig. 6. The vector $\mathbf{q}_{\mathrm{IFF}}$ transformed to the lamina coordinate system becomes vector $\mathbf{q}_2$ in Eq. 32.

The local coupling vector $\mathbf{q}_{\mathrm{IFF}}$ is transformed to the lamina coordinate system as a function of the fracture angle θ_{fp}. Hence the evolution of damage variables $\dot{\boldsymbol{\omega}}$ in the

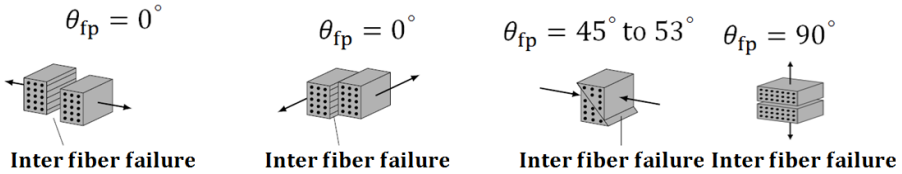

Figure 6: Schematic representation of fracture angle θ_{fp} for various IFF as in Knops (2008).

lamina coordinate system will be according to Eq. 32 without loss of generality:

$$\dot{\boldsymbol{\omega}} = \begin{bmatrix} \dot{\omega}_{11} \\ \dot{\omega}_{22} \\ \dot{\omega}_{33} \\ \dot{\omega}_{12} \\ \dot{\omega}_{23} \\ \dot{\omega}_{13} \end{bmatrix} = \varphi_1 \begin{bmatrix} 1 \\ l_{\parallel\sigma_{22}} \\ l_{\parallel\sigma_{33}} \\ l_{\parallel\tau_{12}} \\ l_{\parallel\tau_{23}} \\ l_{\parallel\sigma\tau_{13}} \end{bmatrix} + \varphi_2 \begin{bmatrix} 0 \\ l_{\perp\sigma_{22}} \\ l_{\perp\sigma_{33}} \\ l_{\perp\tau_{12}} \\ l_{\perp\tau_{23}} \\ l_{\perp\tau_{13}} \end{bmatrix} \tag{37}$$

In the softening range of post critical stress states, the damage growth functions Φ_i are obtained by time integration of ϕ_i in the form of

$$\Phi_i := \int_0^t \phi_i \mathrm{d}\bar{t} = 1 - e^{\frac{1}{m_i}(1-[r_i]^{m_i})}, \; r_i \geq 1 \tag{38}$$

where m_i is the strain softening parameter and r_i is the damage threshold for the criterion g_i at hand. At the onset of failure, triggered by the failure criteria, the value of Φ_i is zero. As the damage progresses, the growth functions Φ_i increase as the damage variables ω_{ij} do, therefore, eventually the stiffness of the material is diminished until a final value of zero is reached.

6 Numerical examples

6.1 Verification example: One element test

In this verification example, a tension test under loading transverse to fibre direction on a UD reinforced laminated composite is presented. The lamina material properties for elasticity are: E_{11}=126 GPa, E_{22}=11 GPa, E_{33}=11 GPa, ν_{12}=0.28, ν_{23} =0.40, ν_{13}=0.28, G_{12}=9 GPa; and for strength: $R_{\perp}^{(+)} = 45$ MPa, $R_{\perp\parallel} = 79$ MPa, $R_{\parallel}^{(+)} = 1950$ MPa. The load is applied in transverse (to fibre) direction until complete failure. Fig. 7 left and Fig. 7 right represents the evolution of damage variables in both original two dimensional (2D) model and the current three

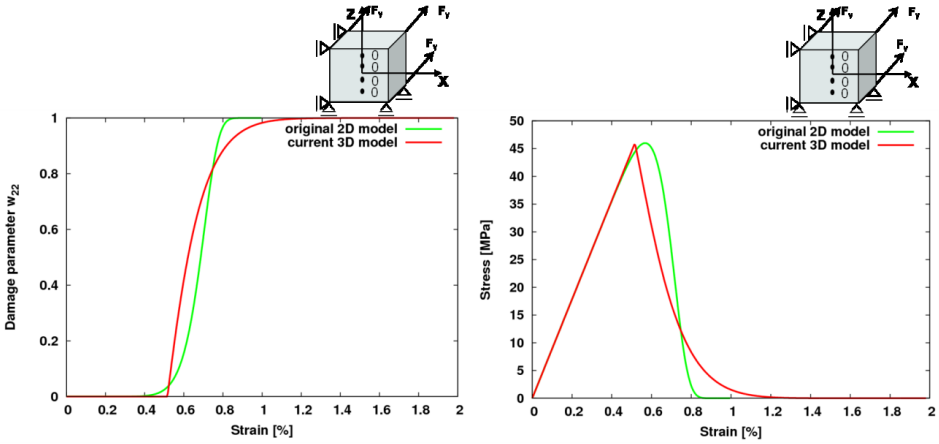

Figure 7: left: Evolution of damage variable ω_{22} in the original 2D model and current 3D model and right: transverse stress-strain curve in both the models

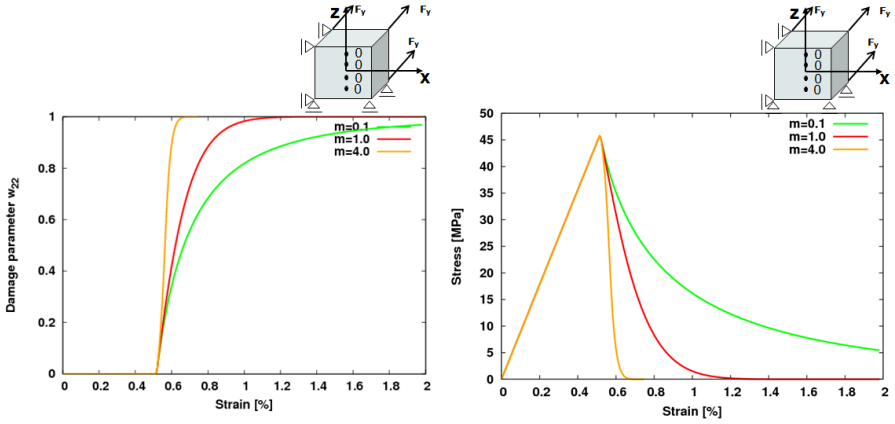

Figure 8: left: Evolution of damage variable ω_{22} with different exponents m and right: Effect of exponent m on the transverse stress-strain curve

dimensional (3D) extension of the model for strain softening exponent $m = 1.0$. Unlike in the original two dimensional model from Matzenmiller, Lubliner and Taylor (1995), where the damage variables effect the stress-strain curves over the entire strain range, in the current model, the damage variables are only applicable to the post-failure part. To avoid strain localization, a smeared formulation similar to Kurnatowski (2010) is utilized. The basic principle of the smeared formulation is the introduction of a length parameter in the damage constitutive law in order

to achieve a constant energy release per unit area of crack generated independent from the element dimensions.

Fig. 8 left and Fig. 8 right represent the evolution of the damage variable and stress vs. strain relationship from the numerical simulation at different exponent m from the current model. It can be seen that the deformation behavior in the loading path remains unchanged with various damage exponent m. After reaching the maximum stress, damage progression is at a faster speed with increasing m, thus representing a more brittle behavior.

6.2 Verification example: Thin-walled tube

The thin-walled, single-layered composite tube in Fig. 9a serves as a second verification example for the meso-level approach with the multi-layered solid element, see Chatiri, Schuetz and Matzenmiller (2010), Fiolka and Matzenmiller (2007). The inner and outer radii of the tube are r_i =16.5 mm and r_a = 18.5 mm with a tube length of l_x = 100 mm. The angle of the filament winding relative to the cylinder axis x_3 is denoted by Θ. The composite consists of the E-glass-fibre reinforced epoxy resin MY750 with a fibre volume content of $v_f = 60\%$. The strength parameters, Puck constants in the failure criteria of Eq. 3 or Eq. 4 and the elasticity moduli of the E-glass-fibre reinforced epoxy resin MY750 are taken from the World-Wide Failure Exercise (WWFE), pp 36, see Soden, Hinton and Kaddour (2004), as well as from Puck and Schürmann (2004), pp 846 and added also to Table 2. The material parameters for nonlinear elastic behavior in-plane shear which is modelled according to the Ramberg-Osgood are identified as σ_0=107 MPa and $n = 9$. The exponent parameter $m = 1.0$ is used for all the simulations below. These parameters are obtained by fitting the numerical stress-strain response to the corresponding experimental data of UD- composite material by performing similar one element UD simulations as in section 6.1. The FE mesh consists of 36 elements in circumferential direction and one element through the thickness of the layer. The tube is discretized by 10 elements in axial direction. Along the boundary at $x_3 = 0$, degrees of freedom for u_3 and u_ϕ are suppressed where u_3 is the axial and u_ϕ the tangential displacement component. The load is applied in terms of prescribed displacements versus time up to a final value of $u_3(l) = 0.3$ mm at the far end of the tube along the edge at $x_3 = l$ in axial direction. The fibres run in circumferential direction ($\Theta = 90^\circ$). Hence, the normal stress caused is perpendicular to the fibres.

Fig. 9b depicts the tensile stress σ_{33} versus the strain $\varepsilon_{33} = u_3(100)/l$ due to the prescribed displacement relative to the tube length $u_3(l)/l$. Up to failure at the stress level of $\sigma_{33}^{\max} = 40$ MPa, the normalized load-displacement is linear. After reaching the strength limit, the stress-strain diagram gradually falls after failure. The results match with the experimental data from WWFE.

Table 2: Parameters for E-glass, epoxy resin MY750 composite

UD-fibre composite strength parameters	$R_{\perp}^{+}$ [MPa]	$R_{\perp\parallel}$ [MPa]	$R_{\perp}^{-}$ [MPa]	$R_{\parallel}^{+}$ [MPa]	$R_{\parallel}^{-}$ [MPa]
	40	73	145	1280	800
Puck constants	$p_{\perp\parallel}^{(+)}$	$p_{\perp\parallel}^{(-)}$	$p_{\perp\perp}^{(\pm)}$		
	0.25	0.3	0.13		
elasticity moduli	$E_{\parallel}$ [GPa]	$E_{\perp}$ [GPa]	$G_{\parallel\perp}$ [GPa]	$\nu_{\parallel\perp}$	$\nu_{\perp\perp}$
	45.6	16.2	5.83*	0.278	0.4
*Note: Nonlinear behavior and stress strain curves and data points are provided.					

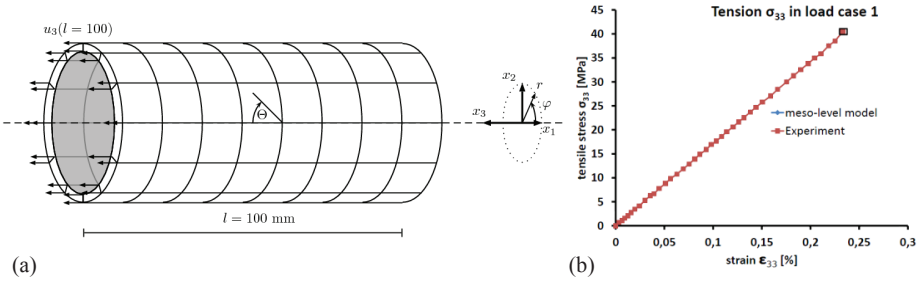

Figure 9: (a) Geometry of thin-walled tube (b) Tension stress σ_{33}vs. strain ε_{33}

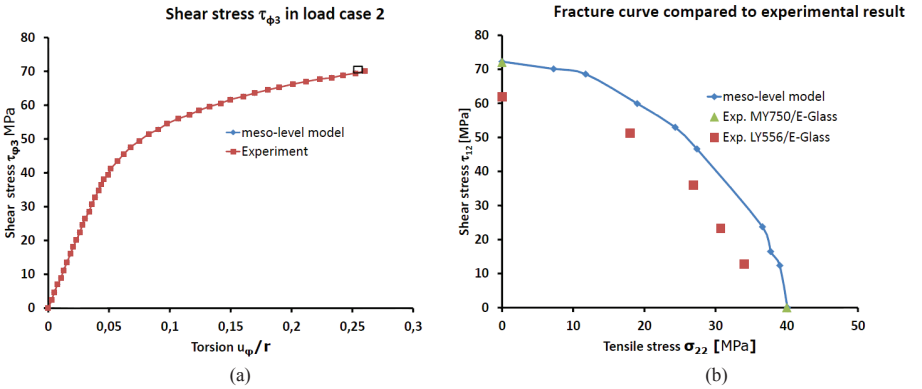

Figure 10: (a) Shear stress $\tau_{\varphi 3}$ vs. Torsion (b) Comparison of Fracture curve

In load case 2, a path-controlled torsional deflection is applied at the far end of the tube. The prescribed deformation causes a homogeneous shear stress in the tube. Hence, the composite is exposed to an axial shear loading due to the fibre orienta-

tion. The load bearing capacity of the tube under torsional loading is reached for the shear stress at $\tau_{3\varphi} \approx 70$ MPa in the implemented meso-level material model compared to an experimental axial shear strength value $R_{\perp\parallel}$ of 73 MPa. In load case 3, combined tension/shear stress loadings are applied and the computed fracture curves are compared to experimental results, see Fig. 10. The experimentally measured strength data for E-glass-fibre reinforced epoxy resin MY750 with a fibre volume content of $v_f = 60\%$ is only available for pure tension and pure shear. For mixed states of biaxial stress, the experimental data points marked by red squares, show the strength data of composite material E-glass/LY556 ($v_f = 62\%$). Both these experimental data sets are diagrammed together in Soden, Hinton and Kaddour (2004) to describe the experimental fracture curve of the composite material E-glass-fibre reinforced epoxy resin MY750 under mixed loading. The numerical results for the strength values, obtained with the current model are close to experimental results.

6.3 Cross-ply laminate under uniaxial tensile loading

The cross-ply laminate with four UD-fibre layers $[0°/90°/90°/0°]$ in Fig. 11 is made of E-glass/MY750 epoxy resin with $v_f = 0.62$ and used to validate the present model. The material parameters are the same as in example 6.2. The test specimen's length is $l_x = 200$ mm, the width $l_y = 25$ mm and the total thickness $l_z = 4 \times 0.475 = 1.9$mm. The fibre orientation in the outer layers coincides with the loading direction. The FE model for the meso-level approach uses one multi-layered 8-node (linear) solid (MLS) element with four integration points to take into account the various fibre orientations given above.

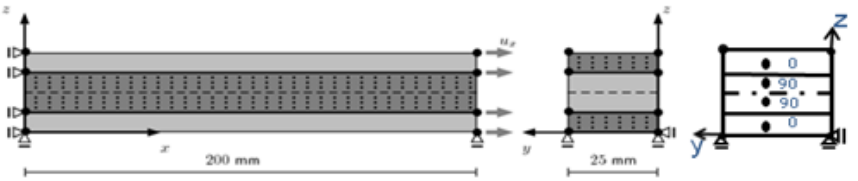

Figure 11: FE-model of cross-ply laminate: longitudinal view, cross section and fibre angles, see Kurnatowski (2010)

The option of representing several plies in one solid element and more such elements across the thickness is implemented into the explicit code, see Hallquist (2010). Like any linear brick element, the MLS resolves the 3D stress state, but may contain n-layers from the composite laminate. It is assumed to be small in

comparison to the overall size of the composite thickness. Its in-plane behavior is treated by through-the-thickness integration, whereas the transverse properties in the shear and normal mode for the hexahedron element must be based on the concept of a homogeneous substitute material, since the underintegrated linear element relies on a uniform membrane stress state. Hence, homogenization of the layer dependent properties is required through the thickness of the element. The homogenization result is bounded by VOIGT's and REUSS's hypotheses, see Voigt (1889), Reuss (1929). The REUSS bound for laminae, connected in series, is close to the effective elasticity modulus in transverse normal direction, whereas the VOIGT bound for laminae, assembled in parallel, serves as an upper limit and approximates the transverse shear modulus of the laminate tightly. Both bounds are implemented into the code to compute the transverse stresses from the strains.

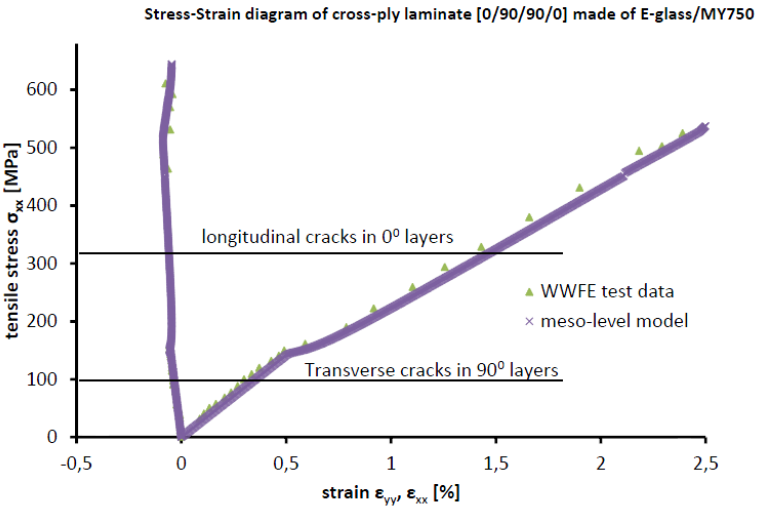

Figure 12: Average stress (σ_{xx})vs. longitudinal $(\varepsilon_{xx})$and transverse strain (ε_{yy})in meso-level model compared to experimental results from Gotsis, Chamis and Minnetyan (2004)

The boundary conditions, imposed on the nodal displacements do not constrain lateral extensions of the specimen. The simulation is controlled by the displacement u_x given at the right end with $l_x = 200$ mm. In Fig. 12, the average laminate stress σ_{xx} is plotted versus the average strain $\varepsilon_{xx} = u_x/l_x$ as well as the lateral average strain $\varepsilon_{yy} = u_y/l_y$ as founded by tests published in Gotsis, Chamis and Minnetyan (2004). At the average longitudinal stress $\sigma_{xx} = 116$ MPa, first cracks perpendicular to the loading direction are observed experimentally in the embedded layer with

fibres in 90°-direction, causing a slight reduction of the laminate's tensile stiffness, represented by the small kink in the stress-strain diagram. At $\sigma_{xx} = 325$ MPa, cracks occur parallel to the loading direction at the outer layers in the test. The damage is due to the tensile stress σ_{yy} resulting from the lateral strain ε_{yy} which is obstructed by the large stiffness of the inner layers in loading direction. At $\sigma_{xx} =$ 600 MPa, final failure of the laminate occurs by tensile fibre fracture in the upper and lower layer.

In the meso-level model, the first transverse cracks in the 90°-layers appear at an average stress level of $\sigma_{xx} \approx 120$ MPa and the longitudinal cracks in the 0°-layers appear at $\sigma_{xx} \approx 340$ MPa. At $\sigma_{xx} \approx 640$ MPa, final failure of the laminate is computed by tensile fibre fracture in the upper and lower layers. It is a matter of common knowledge that the constitutive behavior of a single UD-layer differs from that of the same layer being part of a laminate structure, see Cuntze (2006). Experiments reveal that the embedded lamina withstands higher loading than the isolated one. Hence, underestimating the stiffness and strength of the laminate is not unexpected, if UD-parameters from a single laminae are used for the prediction of the overall behavior of a multilayer composite.

7 Summary and concluding remarks

The meso-level model with the 3D Puck failure criteria and anisotropic continuum damage mechanics is very effective in analyzing multi-layered structures having a large number of plies. The developed material model describes both onset and progression of damage. It can reproduce the key physical aspects observed in the failure of Fibre-reinforced laminated composites. The failure-model implementation is 3D, and allows non-linearity in-plane shear. To avoid strain localization, a smeared formulation is utilized. The numerical implementation has been verified by analysing a single-layered thin-walled tube under homogeneous tensile and shear stress loading. The cross-ply laminate under uniaxial tension is used as the first example for the validation. In general, the simulation results are shown to accurately predict failure envelopes and trend. Further validation has to be done with test data, taken from non-homogenous states of stress in multi-layered composites.

Acknowledgement

The first author gratefully acknowledges financial support and helpful discussions with Drs. Stephan Fell from GM Alternative Propulsion Center Europe, Ruesselsheim, Germany and Matthias Hoermann from CADFEM GmbH, Grafing, Germany.

References

Cauvin, A.; Testa, R. B. (1999): Damage mechanics: basic variables in continuum theories. *Int. J. Solids Struct.*, vol. 36, pp. 747–761.

Chaboche, J. -L. (1995): A continuum damage theory with anisotropic and unilateral damage. *Recher. Aerospat.*, vol. 2, pp. 139–147.

Chatiri, M.; Schuetz, T,; Matzenmiller, A. (2010): An assessment of the new LS-DYNA® multi-layered solid element: basics, patch simulation and its potential for thick composite structural analysis. *Proc. 11^{th} Intl. LS-DYNA® Users Conf.* Detroit, USA.

Cuntze, R. G. (2006): Efficient 3D and 2D failure conditions for UD laminae and their application within the verification of the laminate design. *Composites Science and Technology*, vol. 66, pp. 1081-1096.

Deuschle, H. M.; Kröplin, B. H. (2012): Finite element implementation of Puck's failure theory for fibre-reinforced composites under three-dimensional stress. *J. Composite Materials*, vol. 46, pp. 2485-2513.

Fiolka, M.; Matzenmiller, A. (2007): On the resolution of transverse stresses in solid-shells with a multi-layer formulation. *Commun. Numer. Meth. Engg.*, vol. 23, pp. 313-326.

Fischer, O. (2003): Fibre Fracture Behavior in Fibre Reinforced Plastics. PhD Thesis, RWTH Aachen, Institut für Kunststoffverarbeitung (IKV).

Gotsis, P. K.; Chamis, C. C.; Minnetyan, L. (2004): Application of progressive fracture analysis for predicting failure envelopes and stress-strain behaviors of composite laminates: a comparison with experimental results, in *Failure Criteria in Fibre Reinforced Polymer Composites*: *The World-Wide Failure Exercise*, Soden, P. D.; Hinton, M. J.; Kaddour, A. S., Eds. Elsevier: Oxford, pp. 703-723.

Hallquist, J. O. (2010): *LS-DYNA Theoretical Manual*, Livermore Software Technology Corporation, Livermore, California.

Hashin, Z. (1980): Failure criteria for unidirectional fibre composites. *J. Appl. Mech.*, vol. 47, pp. 329-334.

Ju, J. W. (1989): On energy-based coupled elastoplastic damage theories: constitutive modeling and computational aspects. *Int. J. Solids Struct.*, vol. 25, no. 7, pp. 803-833.

Kachanov, L. M. (1958): Time of the rupture process under creep conditions. *Isv. Akad. Nauk S.S.S.R., Otd. Tekh. Nauk*, vol. 8, pp. 26–31.

Knops, M. (2008): *Analysis of Failure in Fibre Polymer Laminates*: *The Theory of Alfred Puck*. Springer-Verlag: Berlin, Heidelberg.

Kurnatowski, **B.** (2010): Zweiskalensimulation von mikroheterogenen Strukturen aus spröden Faserverbund-werkstoffen, Institut für Mechanik, Fachbereich Maschinenbau, Universität Kassel, Ph. D. Thesis.

Kurnatowski, B.; Matzenmiller, A. (2012): Coupled twoscale analysis of fiber reinforced composite structures with microscopic damage evolution. *Int. J. Solids Struct.*, vol. 49, pp. 2404-2417.

Ladeveze, P.; Allix, O.; Deü, J. -F.; Leveque, D. (2000): A mesomodel for localisation and damage computation in laminates. *Comput. Methods Appl. Mech.* Eng. 183, pp.105–122.

Lubliner, J. (1990): *Plasticity Theory*, Macmillan, Newyork.

Matzenmiller, **A.; Lubliner**, **J.; Taylor**, **R. L.** (1995): A constitutive model for anisotropic damage in fibre composites. *Mechanics of Materials*, vol. 20, pp. 125-152.

Maimí, P.; Camanho, P.P.; Mayugo, J.A.; Dávila, C.G. (2007): A continuum damage model for composite laminates. Part I: Constitutive model. *Mechanics of Materials*, vol. 39, pp. 897-908.

Ortiz, M. (1985): A constitutive theory for the inelastic behavior of concrete. *Mech. Mater.*, vol. 4, pp. 67-93.

Pinho, S. T.; Iannuci, L.; Robinson, P. (2005): Physically based failure models and criteria for laminated fibre-reinforced composites with emphasis on fibre kinking. Part II: FE implementation, *Composites Part A*. vol. 37, pp. 766-777.

Puck, A.; Schürmann, H. (2004): Failure analysis of FRP laminates by means of physically based phenomenological models, in *Failure Criteria in Fibre Reinforced Polymer Composites*: *The World-Wide Failure Exercise*, P. D. Hinton, A. S. Kaddour, and M. L. Soden, Eds. Elsevier: Oxford, pp. 832-876.

Ramberg, W.; Osgood, **W. E.** (1943): Description of stress–strain curves by three parameters. *National Advisory Committee for Aeronautics*, *Technical Note No.*, 902.

Reuss, A. (1929): Berechnung der Fließgrenze von Mischkristallen auf Grund der Plastizitätsbedingung für Einkristalle. *Z. Angew. Math. Mech.*, vol. 9, pp. 49-58.

Rosen, B.W.; Dow, N. E. (1972): Mechanics of failure of fibrous composites, in: H. Liebowitz, ed., *Fracture - An Advanced Treatise*, Academic Press, pp. 661.

Simo, J. C.; Ju, J. W. (1987a): Strain and stress-based continuum damage models-I. Formulat. *Int. J. Solids Struct.*, vol. 23, pp. 821–840.

Simo, J. C.; Ju, J. W. (1987b): Strain and stress-based continuum damage models-II. Comput. Aspects. *Int. J. Solids Struct.*, vol. 23, pp. 841–869.

Soden, P. D.; Hinton, M.J.; Kaddour, A.S. (2004): Lamina properties, lay-up configurations and loading conditions for a range of fibre reinforced composite laminates, in *Failure Criteria in Fibre Reinforced Polymer Composites*: *The World-Wide Failure Exercise*, Soden, P. D.; Hinton, M. J.; Kaddour, A. S., Eds. Elsevier: Oxford, pp. 30-51.

Talreja, R. (1985a): A continuum mechanics characterization of damage in composite materials. *Proc. R. Soc. Lond. A* 399, 195.

Talreja, R. (1985b): Transverse cracking and stiffness reduction in composite laminates. *J. Composite Materials*, vol. 19, pp. 355.

Voigt, W. (1889): Über die Beziehung zwischen den beiden Elastizitätskonstanten isotroper Körper, *Wied. Ann.*, vol. 38, pp. 573-587.

Williams, K.V.; Vaziri, R.; Poursartip, A. (2003): A physically based continuum damage mechanics model for thin laminated composite structures. *Int. J. Solids Struct.*, vol. 40, pp. 2267–2300.